Episodic Subglacial Drainage Outbursts Below the Northeast Greenland Ice Stream

J. K. Andersen[1], N. Rathmann[2], C. S. Hvidberg[2], A. Grinsted[2], A. Kusk[1], J. P. Merryman Boncori[1], and J. Mouginot[3]

[1]DTU Space, Tech. Univ. of Denmark, 2800 Kgs. Lyngby, Denmark
[2]Niels Bohr Institute, Univ. of Copenhagen, 2100 Copenhagen, Denmark
[3]Univ. Grenoble Alpes, CNRS, IRD, Grenoble INP, IGE, 38000 Grenoble, France

Key Points:

- Episodic subglacial drainage of water over a ∼500 km extent along the Northeast Greenland Ice Stream is revealed by radar interferometry
- The drainage events cause transient uplift and ice flow speed-up in downstream regions, and multiple drainage cascades are observed
- Propagation speed of the drainage cascade varies widely along the ice stream, suggesting fundamental differences in basal conditions

Corresponding author: J. K. Andersen, jkvand@space.dtu.dk

Abstract

Subglacial hydrology can exert an important control on ice flow by affecting drag at the ice-bedrock interface. Here, we report on a series of subglacial drainage events (outbursts) along the Northeast Greenland Ice Stream (NEGIS), initiating as far inland as ∼500 km from the margin of Zachariae Isstrøm. The drainage events are associated with local transient uplift, followed by prolonged subsidence, measured by satellite synthetic aperture radar interferometry (DInSAR). In downstream regions, drainage events are associated with a local speed-up in ice flow. The high spatiotemporal resolution of the DInSAR measurements allows for a detailed mapping of the drainage propagation pathway. We show that multiple drainage cascades have occurred along the same identified pathway over the years 2020-2022. Finally, the propagation speed of subglacial water flow is found to vary greatly along NEGIS, suggesting that fundamental differences may exist in the subglacial environment.

Plain Language Summary

The presence of water flowing beneath the Greenland ice sheet impacts the drag exerted on ice flowing from inland to marginal regions, potentially affecting the rate of sea level rise. Direct observations of the hydrological system beneath glaciers are, however, limited due to inaccessibility. Here, we present satellite observations of localized ice uplift and subsidence, which indicate water propagating below the Northeast Greenland Ice Stream, from far inland to a major marine-terminating glacier, Zachariae Isstrøm. In downstream regions, ice flow speeds up as the subglacial water passes. The measurements indicate variations in the local subglacial environment, which provide important constraints for understanding the flow and stability of the ice stream.

1 Introduction

The Northeast Greenland Ice Stream (NEGIS) is a unique feature of the Greenland ice sheet, being the only ice stream with enhanced ice flow 600 km inland from the margin. It is drained by three marine-terminating outlet glaciers: Zachariae Isstrøm (ZI), Nioghalvfjerdsfjorden, and Storstrømmen, collectively draining an area of more than 16% of the Greenland ice sheet and holding a 142 cm sea level equivalent (Mouginot et al., 2019). Frontal changes at ZI occurring in 2012 have resulted in extensive flow acceleration and ice thinning in the downstream regions (Khan et al., 2014; Mouginot et al.,

2015), and recent results indicate that the NEGIS sector alone will contribute 13.5-15.5 mm to sea level rise by 2100 (Khan et al., 2022). Meanwhile, a widening of the ice stream has been observed in upstream NEGIS over the past four decades, which was attributed not to frontal changes but to softening of the shear margins (Grinsted et al., 2022).

Transport of subglacial water has long been observed to occur over large spatial scales in Antarctica, where pooling of water into subglacial lakes and drainage through interconnected drainage pathways has been documented (Fricker et al., 2007; Neckel et al., 2021; Wingham et al., 2006). Analyses based on hydrological potential estimates and radar-echo sounding surveys suggest that basal water and subglacial lakes are likely prevalent under much of the Greenland ice sheet as well, particularly under fast-flowing regions such as NEGIS (Jordan et al., 2018; Livingstone et al., 2013; Oswald et al., 2018). So far, however, substantially fewer observations have been made of subglacial lake activity below the Greenland ice sheet, compared to its Antarctic counterpart (Livingstone et al., 2022), and no observations have been made of drainages beneath fast-flowing glaciers. A recent mapping of subglacial lakes under the Greenland ice sheet, using airborne radar-echo sounding and measurements of surface elevation change, found no indication of lakes in the NEGIS region, although it was stressed that the prior method may have difficulties in separating subglacial lakes from saturated sediments, which are expected to be present at the uniformly thawed bed under NEGIS (Bowling et al., 2019; MacGregor et al., 2022).

In this study, we present a series of episodic subglacial drainage events propagating ∼500 km along the NEGIS over the span of nearly two years. Using interferometric Synthetic Aperture Radar (SAR) measurements of high spatiotemporal resolution, we are able to observe subtle, transient vertical displacements as water propagates through the upstream parts of the ice stream. Furthermore, we show that the drainage events are associated with an increase in ice flow speed once the downstream faster-flowing regions of NEGIS are reached by the subglacial drainage cascade. Finally, we demonstrate that similar cascades have occurred multiple times over the past few years, and argue that interferometric SAR measurements provide a valuable tool for monitoring the dynamic ice response to transient changes in the subglacial hydrological environment, thereby providing potential constraints on basal properties and the subglacial drainage system.

2 Data and Methods

2.1 Sentinel-1 DInSAR motion measurements

The EU Copernicus Sentinel-1 satellites have recorded an extensive archive of SAR images over most of the Greenland ice sheet, including NEGIS, since the launch of the two satellites, S1A (launched in April 2014) and S1B (launched in July 2016, offline since December 2021). The majority of outlet glaciers have been consistently imaged with the lowest possible repeat-pass period (6-days with both satellites operational), allowing for frequent acquisitions of ice motion. In this study, we use Differential SAR Interferometry (DInSAR) to retrieve ice motion measurements of high accuracy and resolution. DInSAR measures motion in the radar line-of-sight (LoS) direction between two acquisitions. As the LoS is slanted towards ground (with incidence angles of 30-45°), DInSAR retrievals are sensitive to vertical as well as horizontal motion. We produced two DInSAR ice velocity time series consisting of all available Interferometric Wide (IW) image pairs with a 6-day temporal baseline during 2016-2021 for one ascending track (T074) and one descending track (T112). Interferometric processing is carried out using the approach described in (Andersen et al., 2020; Kusk et al., 2022). The output LoS velocity maps are calibrated using Ground Control Points in slow-moving regions outside the ice stream (Text S1). In order to reveal transient changes, we subtract a reference LoS velocity field, taken as the pixel-wise median of the full time series, from the retrievals of each track. Assuming a constant ice flow direction across the time series extent, the resulting velocity anomaly maps contain, in principle, both horizontal flow speed change and vertical motion components (projected onto the radar LoS).

To investigate ice flow in fast-flowing downstream regions (where DInSAR is not applicable) we use Sentinel-1 amplitude-based velocity mosaics from NASA MEaSUREs (Joughin, 2021). These mosaics are generated through range and azimuth offset tracking of 6- and 12-day image pairs and are scaled to provide 6-day horizontal (2D) velocity estimates. The estimated standard error of the velocity magnitude is around 10 m/y for these mosaics (Joughin, 2021), substantially higher than that expected of DInSAR measurements, but low enough to detect flow speed changes of a few percent in downstream NEGIS.

2.2 Identifying dynamic response of individual drainage events

For a given point on the ice surface, fully decomposing the 3D displacement field would require three temporally coincident DInSAR acquisitions with linearly independent LoS directions. In the present case, only two different LoS directions can be acquired (tracks 74 and 112) with a temporal overlap of 3.5 days between 6-day pairs from each acquisition geometry. This makes an exact quantitative decomposition impractical. However, since the ground-projections of the ascending and descending LoS vectors differ by ∼140°, sensitivity to horizontal motion varies widely between the two tracks, whereas the similar vertical incidence angles (varying between 30° and 45° in the across-track dimension for both tracks) lead to similar sensitivities to vertical motion (Figure S1). Assuming a constant ice flow direction, the exact sensitivity to a change in horizontal flow speed and vertical displacement can be computed, respectively, for each satellite track (Figure S2). In some cases, this allows us to qualitatively distinguish between these two signals (section 3.2). In other cases, the horizontal component may be assumed negligible (section 3.1).

If a measured LoS velocity anomaly, v_{LoS}, is assumed to arise purely from vertical displacement (over the 6-day temporal baseline, T), the vertical displacement is computed as:

$$d_{\mathrm{vert}} = \frac{v_{\mathrm{LoS}}}{\cos\theta_i} \cdot T \tag{1}$$

where θ_i is the local incidence angle.

In most of the upstream NEGIS region where subglacial drainage events are observed, we interpret all LoS motion anomalies as vertical displacements (see section 3.1). For each of the local uplift events observed in this region, we estimate the subglacial water volume, V_{sub}, consistent with such uplift, simply as:

$$V_{\mathrm{sub}} = \sum_{n}^{N} d_{\mathrm{vert},n} \cdot dx \cdot dy \tag{2}$$

where $dx = dy = 50$ m is the pixel spacing of the DInSAR measurements. The sum is over all pixels affected by uplift, which are defined as pixels with $d_{\mathrm{vert}} > 2.5$ cm (well above the noise floor imposed by calibration errors, which we estimate on the or-

der of 1 cm through measurements in event-free areas). Although calibration errors and other noise sources may bias individual volume estimates, the subglacial water volume time series provides a first order magnitude estimate of the amount of water transported by the drainage cascade. To add further confidence in this calculation, we explored how imposed elastic displacements of the subglacial interface transfer to the surface in an idealized finite-element model (linear elastostatic model with canonical isotropic elastic parameters of ice; not shown). Indeed, when integrating over the displacement field, the volume of the (imposed) subglacial cavity matches the displaced volume of the surface, although height and spatial extent of the anomalies differ between bed and surface.

3 Results

3.1 Propagation of drainage outbursts

Figure 2a shows vertical displacement anomalies inferred from DInSAR measurements in the upstream parts of the study site, indicated by the blue rectangle in Figure 1. In these upstream regions, observed DInSAR LoS velocity anomalies generally consist of small-scale, contiguous polygons, which are not consistent with a change in horizontal flow speed. This is supported by comparing measurements from the descending track (112) to measurements from an additional ascending track (89), suggesting that the observed anomalies are consistent with vertical displacements and not horizontal flow changes (see Figure S3). For individual events in upstream NEGIS, uplift magnitudes are mostly on the order of 5-15 cm (over the 6-day temporal baseline), but for events during 25th July through 12th August, uplift magnitudes exceeding 30 cm (per 6 days) are measured. Note that some areas exhibit uplift through multiple 6-day acquisition cycles. Uplift events are observed to propagate downstream in a bead-and-thread structure, similar to that observed in other recent studies of drainage cascades (Maier et al., 2023; Neckel et al., 2021), with uplift concentrated in polygons with lengths on the order of 5-25 km. Within most of the identified regions of uplift, subsidence of a relatively low magnitude is observed during weeks or months following the original uplift signal. From July 25th, the uplift wave branches out in two components: one propagating further downstream towards the ZI margin, and one propagating eastward, ultimately ending up in the eastern section of the ice stream, also leading to the ZI margin. Polygons in Figure 1a indicate the extent and timing of uplift events occurring in part of the upstream regions.

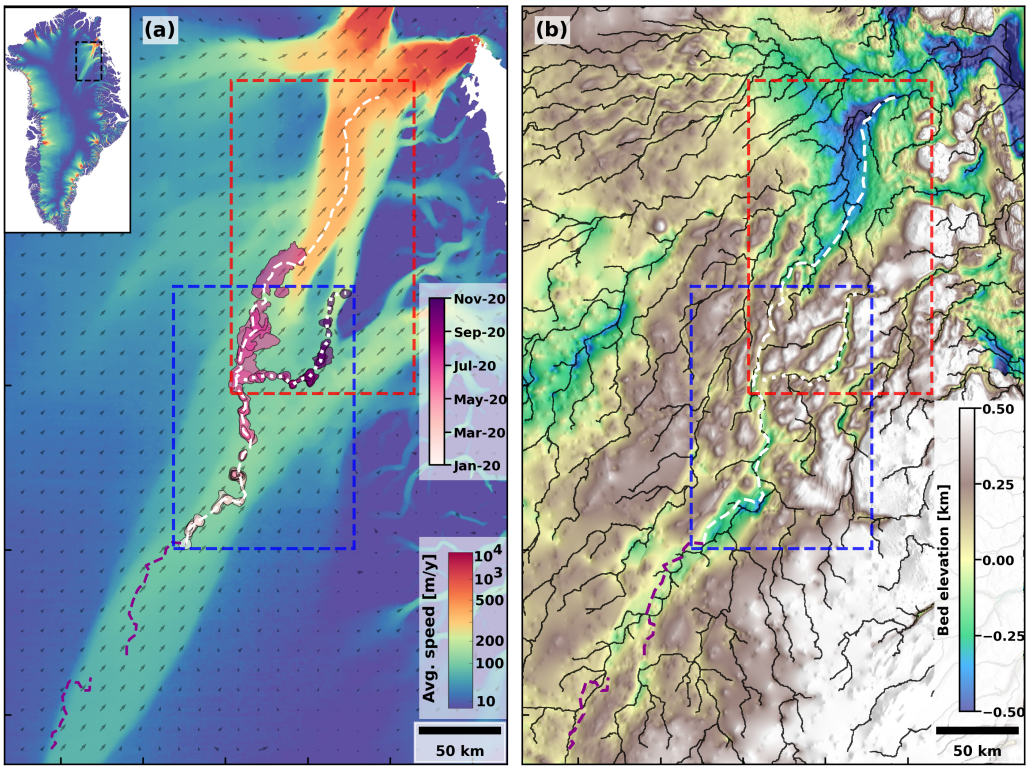

Figure 1. Overview of the NEGIS study site and results. (a) 2016-2019 average velocity magnitude (Solgaard et al., 2021) with gray quivers indicating direction of flow. Polygons indicate extent and timing of some of the localized uplift events identified with Sentinel-1 DInSAR and the dashed/dotted lines indicate propagation pathways followed by the subglacial outbursts observed in 2020 (sections 2.2 and 3.1). (b) Bed elevation (Morlighem, 2021), plotted as a shaded relief. Black lines show flow accumulation pathways based on estimated hydro-potential (section 3.3). Blue and red dashed rectangles indicate extent of plots in Figs. 2a and 2b, respectively.

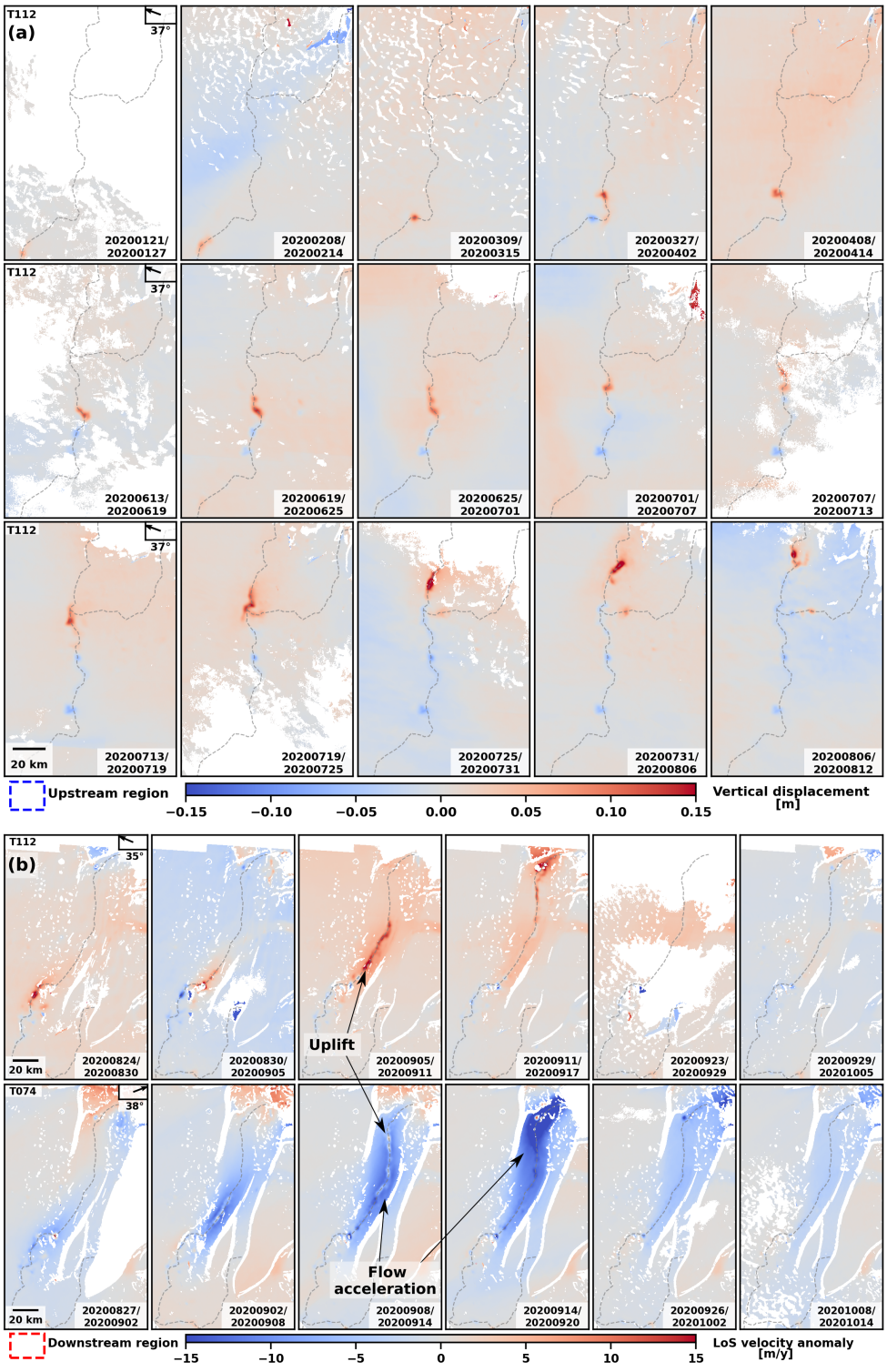

Figure 2. (a) Vertical displacement anomaly maps, inferred from Sentinel-1 DInSAR LoS velocity anomaly measurements (all from descending track 112), covering the upstream NEGIS region (blue rectangle in Figure 1) for different 6-day periods during January to August 2020. (b) DInSAR LoS velocity anomaly maps from Sentinel-1 track 112 (top row) and ascending track 74 (bottom row) covering the downstream NEGIS region (red rectangle in Figure 1). The top right corner of each row's first panel shows the ground-projected LoS direction and incidence angle for the given row. The dashed/dotted lines outline the propagation pathway followed by the observed uplift events (same as white lines in Figure 1).

We interpret the observed uplift wave as arising from a cascading transport of water through the subglacial environment, where water pressure is locally increased to a point above ice overburden pressure. Many of the uplift signals are observed far inland (elevation above ∼1800 m) and outside of surface melt season, suggesting that the subglacial water originates from basal melt, likely caused by some combination of geothermal and frictional heat. The drainage cascade reaches lower elevations during the summer of 2020, meaning that surface melt may have infiltrated the hydrological system through crevasses or supraglacial lake drainages, contributing further to the total subglacial water budget and thus, potentially, the observed uplift.

Figure 3 shows an overview of location, timing, and estimated water volume for uplift events observed along 220 km of the upstream study site. For events further downstream, vertical displacement cannot be quantitatively separated from horizontal flow acceleration (elaborated on in section 3.2), and for events further upstream, the uplift signals tend to fall below the selected signal threshold of 2.5 cm (see Figure S5). For the first ∼150 km, uplift events generally show water volumes of a few million m^3, whereas events in the last 50 km of the transect, occurring during summertime, show substantially higher volumes >15 million m^3. Figure 3 also shows estimates of the propagation speed of uplift events, taken as a proxy for the speed at which subglacial water is transported downstream. We observe that the propagation speed is highly variable. In the first sector (0-50 km), the speed is 0.009 m/s (23.3 km/month), twice as high as in the second sector (∼50-80 km), where uplift events are continuously observed in the same area for two months. From ∼80 km onwards, the estimated propagation speed is two and four times higher than in the first and second sectors, respectively.

3.2 Downstream dynamic response

Figure 2b shows ascending and descending DInSAR LoS velocity anomaly measurements in the downstream part of the study site (within ∼200 km of the Zachariae glacier front, see red dashed rectangle in Figure 1). The measurements suggest that together with the wave of vertical displacements, concentrated in a localized bead-and-thread pattern (indicated by positive anomalies in the LoS velocity for both tracks), a spatially smooth, large-scale wave of LoS velocity anomalies also propagates downstream during early September to early October. Considering the LoS vectors, this smooth anomaly field is consistent with a speed-up in the horizontal ice flow velocity within this part of the ice stream.

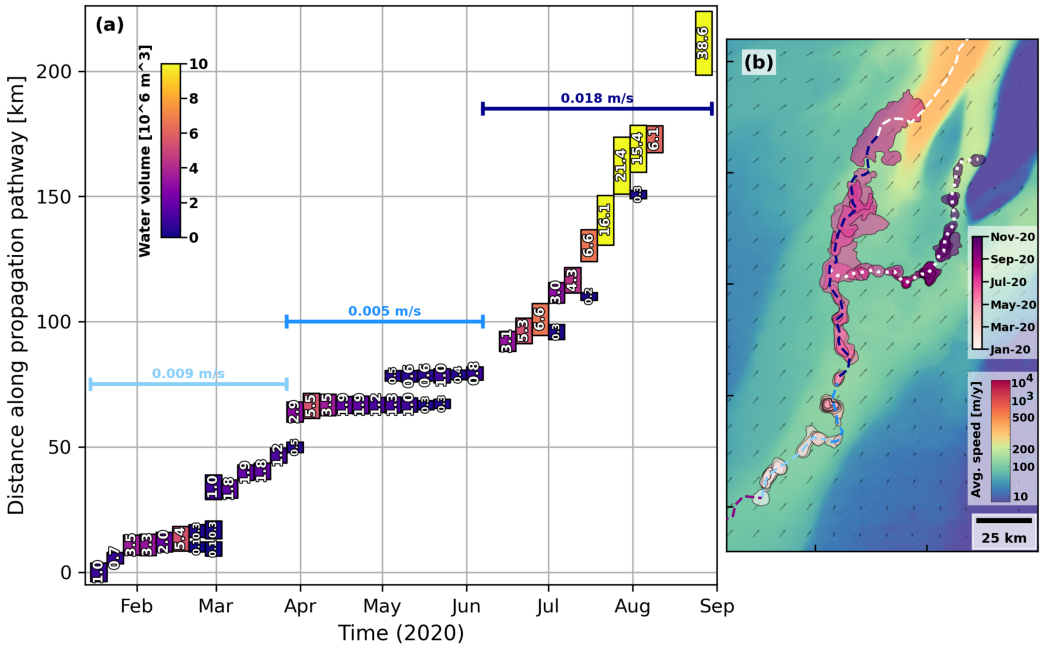

Figure 3. (a) Time series illustrating the occurrence of uplift events along 220 km of the identified propagation pathway (dashed line in (b), same as in Figure 1). Boxes indicate individual uplift events corresponding to the polygons shown in (b), with numbers indicating estimated water volume in 10^6 m^3. The spatial extent of each event is centered on the polygon centroid (projected to the propagation pathway) with the extent defined as the diameter of a circle with an area equal to the polygon area. Estimates of propagation speed of the uplift wave are indicated for different stretches of the pathway (in shades of blue). The corresponding time series for the secondary propagation pathway (dotted white line), is shown in Figure S4.

Indeed, an increase in flow speed is also observed with amplitude-based Sentinel-1 offset tracking measurements. We assembled a time series of the NASA MEaSUREs 2D Sentinel-1 velocity mosaics based on 6- and 12-day Sentinel-1 image pairs from July to November for the years 2018-2021. Interpolating the measurements to a transect along the downstream region reveals that flow speed during 1st-24th September is ∼5% higher than the average speed during October-November; this is not the case in 2018 or 2019, where September flow speed is lower than, or comparable to, October-November values (Figs. 4, S6). The transect in Figure 4 passes through the center part of the ice stream, deliberately avoiding regions of observed uplift, as vertical displacement anomalies are interpreted as horizontal motion in the tracking-based mosaics. Figure S7 illustrates that, for the year 2020, the time of maximum velocity (from July to November) coincides with the September drainage cascade for the final 200 km of ZI (excluding the ∼20 km before the margin, where peak velocity consistently occurs during July-August). For comparison, the same region does not show a clear peak velocity time for the years 2018 and 2019.

As DInSAR coverage is lost about 50 km before the ZI margin, the propagation of uplift events could not be traced in this final stretch. While range offset tracking measurements also have sensitivity to both vertical and horizontal motion, we found that individual 6- and 12-day retrievals did not allow tracking the propagating uplift wave in this region (assuming it exists). However, the MEaSUREs mosaics do indicate an increase in flow speed beyond the DInSAR coverage, suggesting that the drainage cascade may impact ice dynamics far downstream.

3.3 Derived drainage propagation pathways

By manually delineating a path intersecting identified uplift events, a subglacial drainage pathway can be inferred. We delineate the pathway such that it intersects the central parts of the observed uplift events. In many cases, the spatial extent of subsequent uplift events overlap. When this is not the case, subsequent events are connected by the shortest possible straight path. In Figure 1b, the inferred drainage path (white/purple lines) is compared to paths expected from following the negative hydro-potential gradient (black lines; estimated using surface and bed topography from BedMachine v4 (Morlighem, 2021)). Specifically, hydro-potential-derived paths are plotted by calculating the flow accumulation map, which, for a given pixel, indicates the number of upgradient pixels ex-

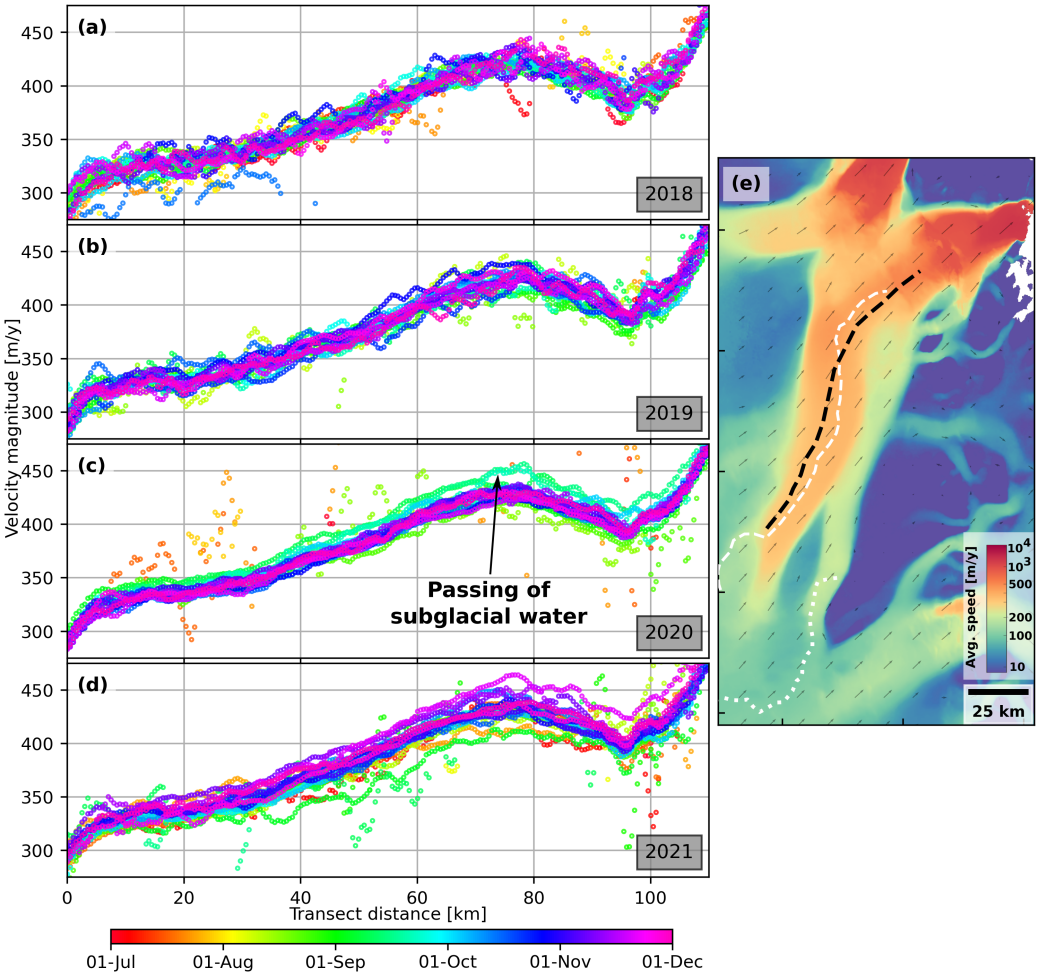

Figure 4. (a)-(d) Horizontal velocity magnitude along the downstream NEGIS transect shown by the black dashed line in (e) for all available Sentinel-1 6-day offset tracking mosaics from NASA MEaSUREs within the period July 1st to December 1st for the years 2018-2021. Data has been spatially averaged using a window size of 1x1 km. In 2018 and 2019, no period shows a consistent maximum in flow speed along the full transect. In 2020, increased flow speeds are observed over the entire transect during September 1st-24th, coincident with the passing of the observed subglacial drainage cascade (see Figure 2). For 2021, peak flow speed is observed during November 18th-30th, coincident with another subglacial drainage cascade (see section 3.4).

pected to drain through that pixel (see Text S2). The DInSAR and hydro-potential-derived pathways closely align in most areas, with the exception of the downstream basal trough, where the paths diverge (see section 4 for further discussion).

3.4 Recurrence of drainage cascades

Investigating the full 2016-2022 DInSAR time series revealed that the drainage cascade described above is not unique. Throughout the time series, other localized incidents of transient uplift and subsidence are observed, both inside and outside of the NEGIS, but do not appear to be associated with changes in ice flow, nor do they propagate for hundreds of kilometers. However, two additional instances of a propagating uplift wave within NEGIS are observed during 2021 and 2022. Figure S8 shows derived vertical displacement anomaly maps covering these events, plotted alongside the propagation pathway observed for the 2020 drainage cascade. The 2021 and 2022 uplift waves appear to closely follow the 2020 pathway. Note, however, that the earliest uplift events in 2021 occur outside of this pathway, before subsequent events coalesce into the previous year's propagation path, all the way downstream, even repeating the split into two branches at exactly the same location as in 2020 (Figure S8, middle row) and the accompanying horizontal flow speed-up (Figure S9). For 2022, DInSAR coverage is severely degraded, particularly downstream, due to the loss of the Sentinel-1B satellite in December 2021. Nonetheless, localized uplift events are observed over parts of the 2020 propagation pathway.

4 Discussion

Direct observations of subglacial drainage below the NEGIS have broad implications for understanding the flow and stability of the ice stream. NEGIS has been suggested to be initiated by a geothermal heat flux anomaly close to the ice divide in central Greenland (Smith-Johnsen et al., 2020; Fahnestock et al., 2001), which is likely the reason for the lack of a developed tributary system to the upstream area of NEGIS (Christianson et al., 2014). The upstream part of NEGIS is thought to be controlled by basal conditions (Keisling et al., 2014; Franke et al., 2021), as there is no distinct bedrock channel (Figure 1b). The pronounced shear margins are marked by troughs in the surface topography, formed by the acceleration and thinning as ice flows into NEGIS (Hvidberg et al., 2020). Christianson et al. (2014) proposed, based on seismic surveys, that these troughs

create gradients in the subglacial hydro-potential that generate wet and dry bands beneath the shear margins. Basal water is directed into the wet, slippery bands beneath the shear margins, and dry, sticky bands within the shear margins are proposed to restrict further widening of NEGIS, thereby stabilizing the ice stream in the upstream area. The first evidence of the episodic drainage outburst observed here did indeed initiate in the shear margin (Figure 1a, purple line) near the study site of Christianson et al. (2014), supporting their hypothesis. Downstream from this first occurrence of the drainage outburst, NEGIS widens as it flows over a bedrock plateau, and the drainage propagates through a basal valley network following the steepest hydro-potential gradient (Figure 1b). It is remarkable that the propagation path is associated with formation of a secondary shear margin that marks a fast flow band within NEGIS (April-June 2020), where depth-average ice-temperature anomalies have also been suggested (Holschuh et al., 2019). The curved water drainage path and complex velocity structure of NEGIS without a distinct bedrock channel (Figure 1), also observed for other Greenlandic ice streams, suggest that NEGIS is not a persistent feature of the northern Greenland drainage basin configuration, which has been proposed to maybe have taken a different configuration earlier in the Holocene (Franke et al., 2022).

It is tempting to speculate whether the magnitude of the (potential) upstream geothermal heat anomaly can be constrained by considering a closed water volume budget, consisting of (say) the upstream geothermal source and shear-margin sources. However, with the limited number of years of detected outbursts, and given the detection limit (signal/noise ratio), such decomposition of the budget does not yet seem possible. As the drainage propagates further downstream, however, the drained water volume grows. Ice deformation and basal sliding generate heat, providing a new source for the growing water volume. Basal melt rates are estimated to be in the order of cm/yr (Smith-Johnsen et al., 2020), but remain poorly constrained. In the downstream part, NEGIS flows into a wide and deep basal trough at more than 500 m below sea level. In this region, passing of the drainage cascade is associated with widespread flow acceleration (Figs. 2b, 4, S7), which would seem to suggest a distributed subglacial flow. The DInSAR measurements, however, show localized uplift/subsidence through this sector, suggesting channelized flow (at least until about 50 km from the ZI margin, where DInSAR coverage is lost). Note that the DInSAR-inferred propagation pathway deviates from the hydro-potential-based drainage pathway in this downstream sector (Fig. 1b).

Basal hydrology is closely linked to sliding and friction at the basal interface (Andrews et al., 2014; Nienow et al., 2017). The characteristics of the observed drainage outbursts suggest that the basal interface between ice, water, and subglacial till evolves in a stick-slip motion, where water is drained by burst-like dynamics. Since upstream NEGIS likely rests on water-saturated till near its onset (Christianson et al., 2014; Franke et al., 2021; Keisling et al., 2014), it is not clear whether the individual outburst events are a result of micro-turbulence in the wetted interface or slower, steady flow through a porous till. Indeed, the different propagation speeds found (Figure 3a) suggest that three different subglacial environments may be present along NEGIS, which could guide future geophysical surveys seeking to (ultimately) observationally constrain different sliding regimes and hence sliding physics.

Data Availability Statement

All data used to generate this manuscript is publicly available. Sentinel-1 data: `https://scihub.copernicus.eu/`, BedMachine bed and surface elevation: `https://doi.org/10.5067/VLJ5YXKCNGXO`, TanDEM-X elevation model: `https://download.geoservice.dlr.de/TDM90/`, PROMICE ice velocity products: `https://dataverse.geus.dk/dataverse/Ice_velocity`, NASA MEaSUREs ice velocity mosaics: `https://doi.org/10.5067/1AMEDB6VJ1NZ`. Line-of-sight anomaly measurements for local uplift events and inferred drainage propagation pathways (indicated by polygons and dashed lines in Figure 1a, respectively) are available at the online repository: `https://doi.org/10.11583/DTU.22060061`. All Figures were produced with Matplotlib version 3.5.0.

Acknowledgments

This work was funded by DTU Space (Technical University of Denmark) and the Independent Research Fund Denmark (DFF), grant no. 2032-00364B. The authors declare no competing interests.

References

Andersen, J. K., Kusk, A., Boncori, J. P. M., Hvidberg, C. S., & Grinsted, A. (2020). Improved Ice Velocity Measurements with Sentinel-1 TOPS Interferometry. *Remote Sensing*, *12*(12), 2014. doi: 10.3390/rs12122014

Andrews, L. C., Catania, G. A., Hoffman, M. J., Gulley, J. D., Lüthi, M. P., Ryser,

C., ... Neumann, T. A. (2014). Direct observations of evolving subglacial drainage beneath the greenland ice sheet. *Nature*, *514*(7520), 80 – 83. doi: 10.1038/nature13796

Bowling, J. S., Livingstone, S. J., Sole, A. J., & Chu, W. (2019). Distribution and dynamics of Greenland subglacial lakes. *Nature Communications*, *10*(1), 2810. doi: 10.1038/s41467-019-10821-w

Christianson, K., Peters, L. E., Alley, R. B., Anandakrishnan, S., Jacobel, R. W., Riverman, K. L., ... Keisling, B. A. (2014). Dilatant till facilitates ice-stream flow in northeast Greenland. *Earth and Planetary Science Letters*, *401*, 57–69. doi: 10.1016/j.epsl.2014.05.060

Fahnestock, M., Abdalati, W., Joughin, I., Brozena, J., & Gogineni, P. (2001). High Geothermal Heat Flow, Basal Melt, and the Origin of Rapid Ice Flow in Central Greenland. *Science*, *294*(5550), 2338–2342. doi: 10.1126/science.1065370

Franke, S., Bons, P. D., Westhoff, J., Weikusat, I., Binder, T., Streng, K., ... Jansen, D. (2022). Holocene ice-stream shutdown and drainage basin reconfiguration in northeast Greenland. *Nature Geoscience*, *15*(12), 995–1001. doi: 10.1038/s41561-022-01082-2

Franke, S., Jansen, D., Beyer, S., Neckel, N., Binder, T., Paden, J., & Eisen, O. (2021). Complex Basal Conditions and Their Influence on Ice Flow at the Onset of the Northeast Greenland Ice Stream. *Journal of Geophysical Research: Earth Surface*, *126*(3). doi: 10.1029/2020JF005689

Fricker, H. A., Scambos, T., Bindschadler, R., & Padman, L. (2007). An Active Subglacial Water System in West Antarctica Mapped from Space. *Science*, *315*(5818), 1544–1548. doi: 10.1126/science.1136897

Grinsted, A., Hvidberg, C. S., Lilien, D. A., Rathmann, N. M., Karlsson, N. B., Gerber, T., ... Dahl-Jensen, D. (2022). Accelerating ice flow at the onset of the Northeast Greenland Ice Stream. *Nature Communications*, *13*(1), 5589. doi: 10.1038/s41467-022-32999-2

Holschuh, N., Lilien, D. A., & Christianson, K. (2019). Thermal Weakening, Convergent Flow, and Vertical Heat Transport in the Northeast Greenland Ice Stream Shear Margins. *Geophysical Research Letters*, *46*(14), 8184–8193. doi: 10.1029/2019GL083436

Hvidberg, C. S., Grinsted, A., Dahl-Jensen, D., Khan, S. A., Kusk, A., Ander-

sen, J. K., ... Vallelonga, P. (2020). Surface velocity of the Northeast Greenland Ice Stream (NEGIS): assessment of interior velocities derived from satellite data by GPS. *The Cryosphere*, *14*(10), 3487–3502. doi: 10.5194/tc-14-3487-2020

Jordan, T. M., Williams, C. N., Schroeder, D. M., Martos, Y. M., Cooper, M. A., Siegert, M. J., ... Bamber, J. L. (2018). A constraint upon the basal water distribution and thermal state of the Greenland Ice Sheet from radar bed echoes. *The Cryosphere*, *12*(9), 2831–2854. doi: 10.5194/tc-12-2831-2018

Joughin, I. (2021). *MEaSUREs Greenland 6 and 12 day Ice Sheet Velocity Mosaics from SAR, Version 1.* NASA National Snow and Ice Data Center DAAC. Retrieved 2023-02-02, from `https://nsidc.org/data/nsidc-0766/versions/1` (Type: dataset) doi: 10.5067/6JKYGMOZQFYJ

Keisling, B. A., Christianson, K., Alley, R. B., Peters, L. E., Christian, J. E., Anandakrishnan, S., ... Jacobel, R. W. (2014). Basal conditions and ice dynamics inferred from radar-derived internal stratigraphy of the northeast Greenland ice stream. *Annals of Glaciology*, *55*(67), 127–137. doi: 10.3189/2014AoG67A090

Khan, S. A., Choi, Y., Morlighem, M., Rignot, E., Helm, V., Humbert, A., ... Bjørk, A. A. (2022). Extensive inland thinning and speed-up of Northeast Greenland Ice Stream. *Nature*. doi: 10.1038/s41586-022-05301-z

Khan, S. A., Kjær, K. H., Bevis, M., Bamber, J. L., Wahr, J., Kjeldsen, K. K., ... Muresan, I. S. (2014). Sustained mass loss of the northeast Greenland ice sheet triggered by regional warming. *Nature Climate Change*, *4*(4), 292–299. doi: 10.1038/nclimate2161

Kusk, A., Andersen, J. K., & Boncori, J. P. M. (2022). Burst Overlap Coregistration for Sentinel-1 TOPS DInSAR Ice Velocity Measurements. *IEEE Geoscience and Remote Sensing Letters*, *19*, 1–5. doi: 10.1109/LGRS.2021.3062905

Kusk, A., Boncori, J. M., & Dall, J. (2018). An automated system for ice velocity measurement from SAR. In *EUSAR 2018 12th European Conference on Synthetic Aperture Radar.* Frankfurt am Main: VDE IEEE.

Livingstone, S. J., Clark, C. D., Woodward, J., & Kingslake, J. (2013). Potential subglacial lake locations and meltwater drainage pathways beneath the Antarctic and Greenland ice sheets. *The Cryosphere*, *7*(6), 1721–1740. doi:

10.5194/tc-7-1721-2013

Livingstone, S. J., Li, Y., Rutishauser, A., Sanderson, R. J., Winter, K., Mikucki, J. A., ... Sole, A. J. (2022). Subglacial lakes and their changing role in a warming climate. *Nature Reviews Earth and Environment*, *3*(2), 106 – 124. doi: 10.1038/s43017-021-00246-9

MacGregor, J. A., Chu, W., Colgan, W. T., Fahnestock, M. A., Felikson, D., Karlsson, N. B., ... Studinger, M. (2022). GBaTSv2: a revised synthesis of the likely basal thermal state of the Greenland Ice Sheet. *The Cryosphere*, *16*(8), 3033–3049. doi: 10.5194/tc-16-3033-2022

Maier, N., Andersen, J. K., Mouginot, J., Gimbert, F., & Gagliardini, O. (2023). Wintertime supraglacial lake drainage cascade triggers large-scale ice flow response in Greenland. *Geophysical Research Letters*. doi: 10.1029/2022GL102251

Morlighem, M. (2021). *IceBridge BedMachine Greenland, Version 4.* NASA National Snow and Ice Data Center DAAC. Retrieved 2023-02-02, from `https://nsidc.org/data/IDBMG4/versions/4` (Type: dataset) doi: https://doi.org/10.5067/VLJ5YXKCNGXO

Mouginot, J., Rignot, E., Bjørk, A. A., van den Broeke, M., Millan, R., Morlighem, M., ... Wood, M. (2019). Forty-six years of Greenland Ice Sheet mass balance from 1972 to 2018. *Proceedings of the National Academy of Sciences*, *116*(19), 9239–9244. doi: 10.1073/pnas.1904242116

Mouginot, J., Rignot, E., Scheuchl, B., Fenty, I., Khazendar, A., Morlighem, M., ... Paden, J. (2015). Fast retreat of Zachariae Isstrom, northeast Greenland. *Science*, *350*(6266), 1357–1361. doi: 10.1126/science.aac7111

Neckel, N., Franke, S., Helm, V., Drews, R., & Jansen, D. (2021). Evidence of Cascading Subglacial Water Flow at Jutulstraumen Glacier (Antarctica) Derived From Sentinel-1 and ICESat-2 Measurements. *Geophysical Research Letters*, *48*(20). doi: 10.1029/2021GL094472

Nienow, P. W., Sole, A. J., Slater, D. A., & Cowton, T. R. (2017). Recent Advances in Our Understanding of the Role of Meltwater in the Greenland Ice Sheet System. *Current Climate Change Reports*, *3*(4), 330–344. doi: 10.1007/s40641-017-0083-9

Oswald, G. K. A., Rezvanbehbahani, S., & Stearns, L. A. (2018). Radar evidence

of ponded subglacial water in Greenland. *Journal of Glaciology*, *64*(247), 711–729. doi: 10.1017/jog.2018.60

Rizzoli, P., Martone, M., Gonzalez, C., Wecklich, C., Borla Tridon, D., Bräutigam, B., ... Moreira, A. (2017, October). Generation and performance assessment of the global TanDEM-X digital elevation model. *ISPRS Journal of Photogrammetry and Remote Sensing*, *132*, 119–139. doi: 10.1016/j.isprsjprs.2017.08.008

Schwanghart, W., & Scherler, D. (2014). Short Communication: TopoToolbox 2 – MATLAB-based software for topographic analysis and modeling in Earth surface sciences. *Earth Surface Dynamics*, *2*(1), 1–7. doi: 10.5194/esurf-2-1-2014

Shreve, R. L. (1972). Movement of Water in Glaciers. *Journal of Glaciology*, *11*(62), 205–214. doi: 10.1017/S002214300002219X

Smith-Johnsen, S., de Fleurian, B., Schlegel, N., Seroussi, H., & Nisancioglu, K. (2020). Exceptionally high heat flux needed to sustain the Northeast Greenland Ice Stream. *The Cryosphere*, *14*(3), 841–854. doi: 10.5194/tc-14-841-2020

Solgaard, A., Kusk, A., Merryman Boncori, J. P., Dall, J., Mankoff, K. D., Ahlstrøm, A. P., ... Fausto, R. S. (2021). Greenland ice velocity maps from the promice project. *Earth System Science Data*, *13*(7), 3491–3512. doi: 10.5194/essd-13-3491-2021

Wingham, D. J., Siegert, M. J., Shepherd, A., & Muir, A. S. (2006). Rapid discharge connects Antarctic subglacial lakes. *Nature*, *440*(7087), 1033–1036. doi: 10.1038/nature04660